NeuroImage 198 (2019) 150–159

Contents lists available at ScienceDirect

NeuroImage

journal homepage: www.elsevier.com/locate/neuroimage

The effects of psychiatric history and age on self-regulation of the default mode network

Stavros Skouras [a,b,*], Frank Scharnowski [c,d,e,f]

[a] Neuroimaging Unit, Barcelonaβeta Brain Research Center, Pasqual Maragall Foundation, Barcelona, 08005, Spain
[b] Department of Experimental and Health Sciences, Pompeu Fabra University, Barcelona, 08005, Spain
[c] Department of Psychiatry, Psychotherapy and Psychosomatics, Psychiatric Hospital, University of Zürich, Zürich, 8032, Switzerland
[d] Neuroscience Center Zürich, University of Zürich and Swiss Federal Institute of Technology, Zürich, 8057, Switzerland
[e] Zürich Center for Integrative Human Physiology (ZIHP), University of Zürich, Winterthurerstr. 190, Zürich, 8057, Switzerland
[f] Department of Basic Psychological Research and Research Methods, Faculty of Psychology, University of Vienna, Liebiggasse 5, 1010 Vienna, Austria

ARTICLE INFO

Keywords:
Learning
Neurofeedback
Rt-fMRI
ECM

ABSTRACT

Real-time neurofeedback enables human subjects to learn to regulate their brain activity, effecting behavioral changes and improvements of psychiatric symptomatology. Neurofeedback up-regulation and down-regulation have been assumed to share common neural correlates. Neuropsychiatric pathology and aging incur suboptimal functioning of the default mode network. Despite the exponential increase in real-time neuroimaging studies, the effects of aging, pathology and the direction of regulation on neurofeedback performance remain largely unknown. Using real-time fMRI data shared through the Rockland Sample Real-Time Neurofeedback project ($N = 136$) and open-access analyses, we first modeled neurofeedback performance and learning in a group of subjects with psychiatric history ($n_a = 74$) and a healthy control group ($n_b = 62$). Subsequently, we examined the relationship between up-regulation and down-regulation learning, the relationship between age and neurofeedback performance in each group and differences in neurofeedback performance between the two groups. For interpretative purposes, we also investigated functional connectomics prior to neurofeedback. Results show that in an initial session of default mode network neurofeedback with real-time fMRI, up-regulation and down-regulation learning scores are negatively correlated. This finding is related to resting state differences in the eigenvector centrality of the posterior cingulate cortex. Moreover, age correlates negatively with default mode network neurofeedback performance, only in absence of psychiatric history. Finally, adults with psychiatric history outperform healthy controls in default mode network up-regulation. Interestingly, the performance difference is related to no up-regulation learning in controls. This finding is supported by marginally higher default mode network centrality during resting state, in the presence of psychiatric history.

1. Introduction

Neuroimaging research is contributing considerably to progress towards the apprehension of neurological and psychiatric disorders, by illustrating and characterizing their neural substrates. Current translational efforts are focused on validating non-invasive, neuroimaging-based diagnostic and therapeutic clinical applications. Out of the most innovative technological developments of our time, neurofeedback (NF) based on real-time functional magnetic resonance imaging (rt-fMRI) enables human subjects to learn to self-regulate their brain function, effecting behavioral changes and improvements of clinical symptomatology (Sitaram et al., 2017). Numerous recent studies have demonstrated therapeutic effects of rt-fMRI NF training on chronic pain (deCharms et al., 2005), addiction (Li et al., 2013; Hartwell et al., 2013), Parkinson's disease (Subramanian et al., 2011), stroke (Robineau et al., 2017; Liew et al., 2016), tinnitus (Haller et al., 2010) and depression (Linden et al., 2012; Young et al., 2014, 2017); consolidating the view that patients can learn to normalize abnormal patterns of brain activity that are associated with pathology (Sitaram et al., 2017; Stoeckel et al., 2014). Nevertheless, knowledge on the precise mechanisms underpinning the self-regulation of brain function is only nascent at present and no conclusive theoretical framework for NF learning has been established (Sitaram et al., 2017). Especially in the context of clinical NF applications, the field is still lacking fundamental empirical evidence.

* Corresponding author. Barcelonaβeta Brain Research Center, Carrer de Wellington 30, 08005, Barcelona, Spain
E-mail addresses: sskouras@barcelonabeta.org, stavros.skouras@uib.no (S. Skouras).

https://doi.org/10.1016/j.neuroimage.2019.05.008
Received 14 June 2018; Received in revised form 22 April 2019; Accepted 3 May 2019
Available online 16 May 2019

First, it has not been ascertained whether individuals with a history of psychiatric pathology are generally expected to perform equally to healthy participants in self-regulating brain function. Second, the way in which psychiatric pathologies affect specific cognitive requirements of a regulation task is unknown. Third, key performance constraints, such as the effect of age, in relation to self-regulation of brain function and pathology, have not been investigated.

Here we address these three open issues regarding self-regulation of brain function, using the largest publicly available rt-fMRI NF repository, comprising data from healthy participants and psychiatric patients, during bidirectional self-regulation of the default mode network (DMN). The DMN is a large-scale cerebral network (Raichle et al., 2001) associated with a variety of brain functions, including perception (Kelly et al., 2008), attention (Weissman et al., 2006), semantic processing (Binder et al., 2009; Krieger-Redwood et al., 2016; Murphy et al., 2017), divergent thinking (Benedek et al., 2016), self-generation of emotion (Engen et al., 2017) and memory (Mayer et al., 2010; Rugg and Vilberg, 2013; Konishi et al., 2015; Murphy et al., 2018; Spreng et al., 2014; Vatansever et al., 2015), which has become highly relevant for clinical applications (Zhang and Raichle, 2010; Brakowski et al., 2017; Mulders et al., 2015; Hamilton et al., 2015). Similarly to psychiatric pathology, aging also incurs suboptimal functioning of the human brain's DMN (Whitfield-Gabrieli and Ford, 2012; Damoiseaux et al., 2008). Recent studies have demonstrated that DMN activity can be modulated through NF training (Harmelech et al., 2013; Megumi et al., 2015; Van De Ville et al., 2012). Thus, the DMN provides an optimal neural substratum for investigating the generic self-regulation of brain function.

Based on previous work assuming common neural mechanisms for up-regulation and down-regulation (Emmert et al., 2016) and proposing a generic neurofeedback learning network (Sitaram et al., 2017), we hypothesized that up-regulation and down-regulation learning scores would be positively correlated. Due to previously noted aberrant DMN function in pathological populations (Whitfield-Gabrieli and Ford, 2012), we expected that healthy participants would perform better than psychiatric patients in DMN self-regulation. Because of the impeding effects of aging on DMN function (Damoiseaux et al., 2008), we predicted that age would show a negative correlation with DMN self-regulation performance.

2. Materials and methods

2.1. Participants

Young adults, aged 20–45 years ($M = 30.94$ years, $SD = 7.32$, $N = 140$; 58% female), took part in the study. Participants were residents of the Rockland County (New York, U.S.A.) and participated voluntarily in the Rockland Sample Real-Time Neurofeedback project, a large study aiming to create a sample with extensive neuropsychological and medical profiling, including several functional neuroimaging tasks (McDonald et al., 2017; Nooner et al., 2012). In order to include participants with a range of clinical and sub-clinical symptoms, minimally restrictive exclusion criteria were applied to exclude individuals with severe illnesses that would compromise compliance with experimental instructions (e.g. history of neoplasia requiring intrathecal chemotherapy or focal cranial irradiation, Global Assessment of Function <50, history of psychiatric hospitalization, or suicide attempts requiring medical intervention). Clinical diagnoses were determined prior to inclusion in the study, by a psychiatrist using SCID-IV criteria (McDonald et al., 2017). Modal psychiatric diagnoses were substance abuse and major depressive disorder, with a high percentage of comorbidity (Fig. 1, Table 1). All subjects gave written informed consent; Institutional Review Board Approval was obtained for this project at the Nathan Kline Institute and at Montclair State University (Nooner et al., 2012). Subjects that presented a past or ongoing psychiatric diagnosis comprised the pathological group ($M = 30.70$ years; $SD = 7.17$; $n_a = 74$; 55.4% female; 89.2% dextrous); subjects that had not presented any psychiatric diagnosis comprised the control group ($M = 30.71$ years; $SD = 7.48$; $n_b = 62$; 50% female; 90.3% dextrous); and four unclassified subjects were excluded from further analysis.

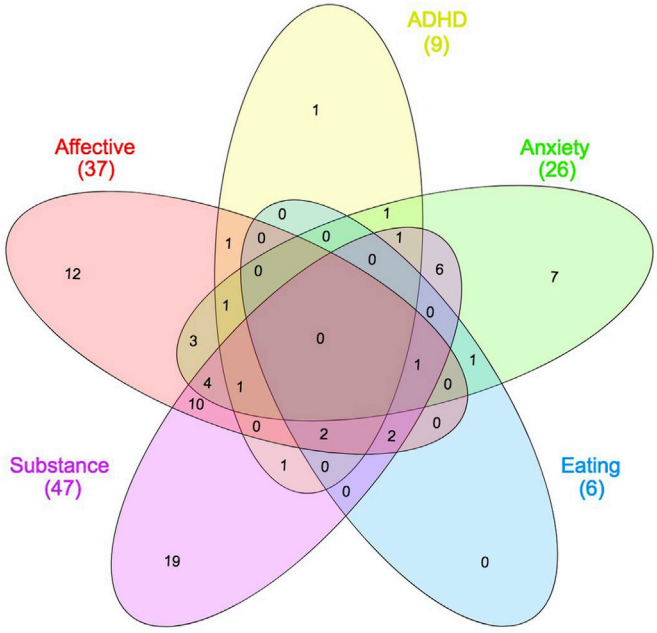

Fig. 1. Comorbidity of primary and secondary clinical diagnoses.
Venn diagram illustrating the total number of cases for each category of disorders and detailing cases of comorbid pathology involving disorders from different categories. Visualization performed using InteractiVenn (Heberle et al., 2015). Color coding is in concordance with Fig. 6: pink ~ affective disorders; yellow ~ ADHD; green ~ anxiety disorders; blue ~ eating disorders; purple ~ substance use disorder.

2.2. Experimental design

Participants completed a variety of assessments and functional neuroimaging tasks comprising the Enhanced Nathan Kline Institute-Rockland Sample (NKI-RS) protocol, described in detail elsewhere (McDonald et al., 2017; Nooner et al., 2012). The protocol included a 6-min resting state fMRI acquisition, followed by a 12-min neurofeedback task. Combined with diagnostic and demographic information, these two acquisitions comprised the only datasets of relevance to the present study. Rt-fMRI data were used to derive neurofeedback performance and neurofeedback learning scores for each participant and for each direction of regulation, via General Linear Modeling (GLM).

Correlation testing was utilized to investigate the relation between DMN up-regulation neurofeedback learning and DMN down-regulation learning scores in the entire sample. Permutation testing was utilized to investigate differences in neurofeedback performance between the experimental group and the control group, for each direction of regulation. Nonparametric correlation testing was used to investigate the relation between neurofeedback performance and age, in each group.

To control for *Type I* error due to performing five individual statistical tests using data from the same sample, we used the Bonferonni correction method (Abdi, 2007) to adjust the typical significance level, $\alpha = 0.05$ (see Statistical analysis). For the typical *Type II* error rate ($\beta = 0.2$), a priori computations of required sample size, using statistical power estimation software (G*Power v 3.1; Heinrich-Heine-Universität Düsseldorf RRID:SCR_013726; Faul et al., 2007; Faul et al., 2009), confirmed sufficient two-tail statistical power for effects of medium or large size using the entire sample ($d > 0.487$) and for effects of moderate or large size using only the pathological group ($d > 0.660$) or only the control group ($d > 0.727$).

Table 1
Prevalence of clinical diagnoses in the pathological group. Specific diagnoses were grouped into five main categories for visualization purposes. Group counts differ from Fig. 1 because many participants were diagnosed with more than one specific diagnosis from the same disorder category (or other disorder categories).

Disorder category	Specific diagnosis	Count
Affective		**38**
	Major Depressive Disorder Single Episode In Full Remission	14
	Major Depressive Disorder Recurrent In Full Remission	12
	Major Depressive Disorder Single Episode Unspecified	4
	Major Depressive Disorder Recurrent Moderate	3
	Dysthymic Disorder	2
	Bereavement	2
	Major Depressive Disorder Recurrent Severe Without Psychotic Features	1
ADHD		**10**
	Attention-Deficit/Hyperactivity Disorder Predominantly Inattentive Type	4
	Attention-Deficit/Hyperactivity Disorder Combined Type	2
	Attention-Deficit/Hyperactivity Disorder NOS	3
	Attention-Deficit/Hyperactivity Disorder Predominantly Hyperactive-Impulsive Type	1
Anxiety		**31**
	Posttraumatic Stress Disorder	7
	Specific Phobia	6
	Generalized Anxiety Disorder	4
	Anxiety Disorder NOS	3
	Panic Disorder With Agoraphobia	3
	Obsessive-Compulsive Disorder	2
	Social Phobia	2
	Panic Disorder Without Agoraphobia	2
	Agoraphobia Without History of Panic Disorder	2
Eating		**6**
	Body Dysmorphic Disorder	2
	Anorexia Nervosa	2
	Bulimia Nervosa	1
	Eating Disorder NOS	1
Substance		**72**
	Alcohol Abuse	26
	Alcohol Dependence	9
	Cannabis Abuse	12
	Cannabis Dependence	12
	Cocaine Abuse	3
	Cocaine Dependence	3
	Amphetamine Abuse	1
	Amphetamine Dependence	1
	Hallucinogen Abuse	1
	Hallucinogen Dependence	1
	Sedative Hypnotic or Anxiolytic Dependence	1
	Opioid Abuse	1
	Polysubstance Dependence	1

2.3. Resting state and neurofeedback task

A resting state acquisition preceded the neurofeedback task because it was required for the delineation of each participant's DMN. During resting state, participants fixated on a white plus (+) sign centered on a black background for 6 min. During the neurofeedback task, stimuli comprised of the neurofeedback display illustrated in Fig. 2B, which was implemented using a programming library (Vision Egg RRID:SCR_014589; Straw, 2008) and is publicly available online from the 'OpenCogLab Repository' (GitHub; RRID:SCR_002630; https://git.io/vptev). All subjects participated in 12 counterbalanced, alternating trials of DMN up-regulation and down-regulation, of varying length (30 s, 60 s, 90 s). Each type of trial (e.g. up-regulation for 30 s) was repeated twice, once in the first and once in the second block of the session. Participants were instructed at the beginning of each trial to attempt to either let their mind wander (up-regulation), or to focus their attention (down-regulation), while attending to one out of four counterbalanced NF displays (Fig. 2A). Counterbalancing was performed with regards to the following: 1) each trial featured a duration of either 30s, 60s or 90s; 2) each trial featured a central instruction, which was either "Focus" or "Wander"; 3) each trial featured the words "Focused" on the left and the word "Wandering" on the right or vice versa.

2.4. MRI data acquisition

Scanning was performed with a 3 T S Magnetom TIM Trio scanner (Siemens Medical Solutions, Malvern, PA, USA) using a 12-channel head coil. Before the functional MR measurements, a fast localizer and high-resolution anatomical sequence were acquired. Anatomical images were acquired using a 3D T1-weighted MPRAGE (Mugler and Brookeman, 1990) GRAPPA (Griswold et al., 2002) sequence with an acceleration factor of 2 and 32 reference lines. 192 sagittal partitions were acquired, each of a 256×256 field of view (FOV), using a 2600 ms repetition time (TR), a 3.02 ms echo time (TE), 900 ms inversion time (TI) and 8° flip angle (FA), resulting in a 1 mm^3 isomorphic voxel resolution.

Functional scanning included a 6-min resting state, comprised of 182 vol and a 12-min neurofeedback task, comprised of 412 volumes. The resting state scan was performed before the neurofeedback task and both scanning sequences featured the same scanning parameters. The overall acquisition protocol featured additional functional tasks (e.g. moral dilemma task; McDonald et al., 2017), which were of no relevance to the present study. Functional images were acquired using echo planar imaging (EPI) with a TE of 30 ms, FA 90° and a TR of 2010 ms. Slice-acquisition was interleaved within the TR interval. The matrix acquired was 64×64 voxels with a FOV of 220 mm, resulting in an in-plane resolution of 3.4×3.4 mm^2. Slice thickness was 3.6 mm with an inter-slice gap of 0.36 mm (30 slices). Images were exported over a network interface (Cox et al., 1995; LaConte et al., 2007). Physiological measures including galvanic skin response, pulse oximetry, rate of breathing and depth of breathing were measured during functional acquisitions.

2.5. MRI data processing

Prior to the NF session, the DMN of each participant had been delineated, based on the data from the resting state scan, using standard fMRI data preprocessing (McDonald et al., 2017) and Support Vector Regression (SVR) with the 3dsvm tool (LaConte et al., 2005), which is based on the SVMlight implementation of machine learning (Joachims, 1999). The procedure used a whole-brain template of the DMN derived from independent component analysis of the 29,671-subject BrainMap activation database (Smith et al., 2009; Fox and Lancaster, 2002; Laird et al., 2005) to extract a weighted timeseries of DMN activity from the resting state data of each participant. The DMN timeseries and the resting state data of each participant were submitted to 3dsvm (similarly to Craddock et al., 2013) resulting in a customized DMN mask for each participant (McDonald et al., 2017). Prior to the NF task, the whole-brain DMN template (Smith et al., 2009) had been used to compute normalization transforms between the native space of each participant's anatomical acquisition and the MNI stereotactic space. This facilitated denoising during the neurofeedback task, when white matter and cerebrospinal fluid signals were regressed out of the rt-fMRI data and the SVR model, that was pre-trained on the resting state data, was used to estimate the DMN activation of each participant, for each real-time TR, using 3dsvm combined with other software routines from AFNI (Analysis of Functional NeuroImages v 18.1.05; National Institute of Mental Health RRID:SCR_005927; Cox, 1996; LaConte et al., 2005) and FSL (FMRIB Software Library v 5.0; Oxford Centre for Functional MRI of the Brain RRID:SCR_002823; Zhang et al., 2001; Jenkinson et al., 2002; Jenkinson and Smith, 2001; Greve and Fischl, 2009; Greve and Fischl, 2009). A two-stage approach was used for motion correction whereby images were coregistered to the mean fMRI volume and then a new mean volume was calculated and used as the target for a second coregistration using AFNI

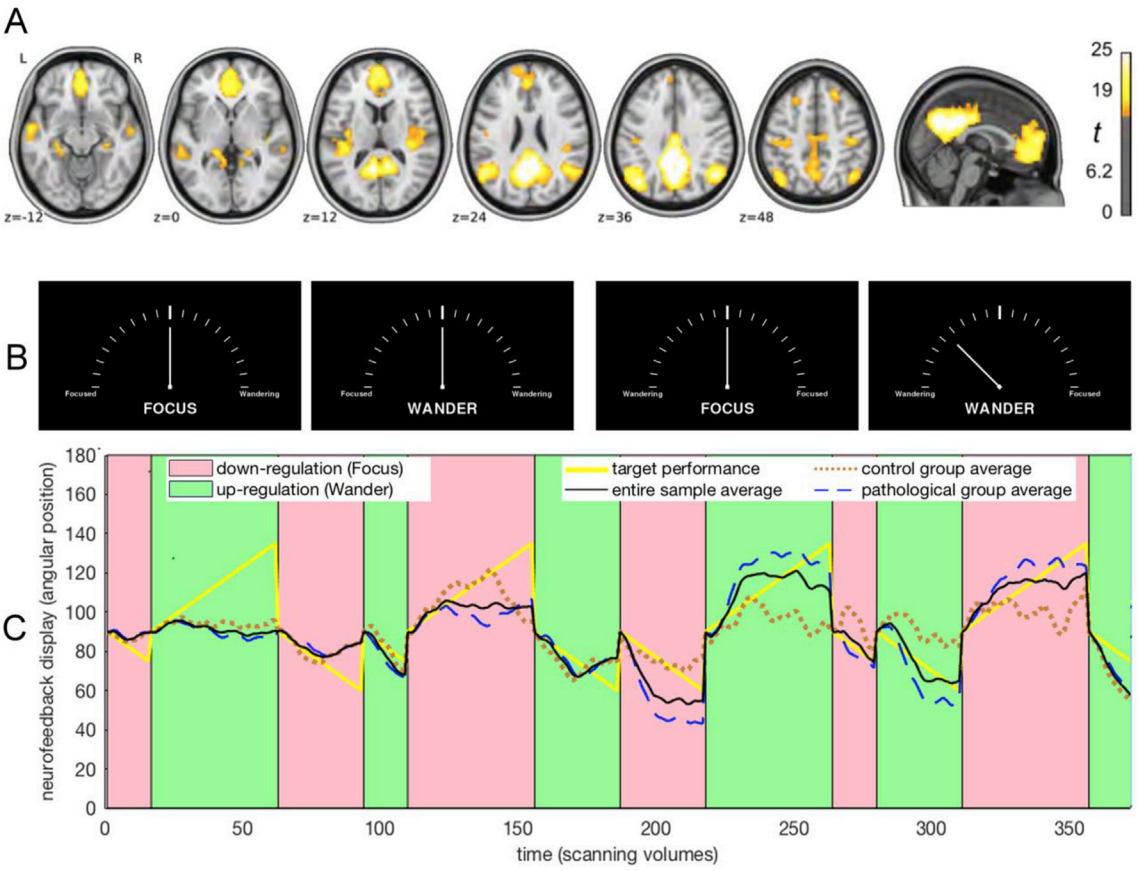

Fig. 2. Modeling regulation performance.
A, Spatial map of the average default mode network in the utilized repository (reprinted with permission, from McDonald et al., 2017). **B**, Each experimental trial featured one of the four counterbalanced displays resembling tachometers. At the beginning of each trial, the angular position of the needle pointer was set to 90° and was updated with every new functional volume according to real-time regulation performance; e.g. the rightmost display shows an angular position of 135°. **C**, The graph shows the average default mode network neurofeedback regulation performance for the pathological group (dashed blue line; N = 74), for the control group (dotted brown line; N = 62) and for the entire sample (black line; N = 136), against target performance (yellow line), in one of four counterbalanced trial orders. It is apparent that on average, learning occurred for both up-regulation and down-regulation and that performance improved noticeably in the second half of the real-time fMRI scanning session.

3dvolreg (Turner et al., 2003; McDonald et al., 2017). Following discretization, the real-time estimates of DMN activation produced by 3dsvm were converted to angular positions of a needle on a tachometer-like NF display, according to four experimental designs that were counterbalanced across participants (Fig. 2B).

All neuroimaging data had been subjected to the 'Preprocessed Connectomes Project Quality Assessment Protocol' (GitHub; RRID:SCR_002630; https://git.io/vptfA; Shehzad et al., 2015) to compute spatial and temporal quality measures, in order to validate or discard acquisitions. Data had been curated on and were accessed via the Collaborative Informatics and Neuroimaging Suite Data Exchange (COINS; Mind Research Network RRID:SCR_000805; Scott et al., 2011; Wood et al., 2014). The data featured a neurofeedback logfile for each participant, summarizing the measures of moment-to-moment neurofeedback performance derived by the real-time processing pipeline that was applied during data acquisition. The neurofeedback logfile for each participant was programmatically retrieved and read into computer memory using software (Matlab v 9.3; Mathworks RRID:SCR_001622). Structured variables were constructed to store all relevant information, regarding each participant's and each trial's characteristics. Hypothesis testing was performed as described in section 'Statistical analysis' and as illustrated in complete detail in the publicly available computer program developed for the analysis (see Code accessibility).

To investigate DMN connectivity patterns at baseline, the DMN template that was also used in the real-time NF pipeline (Smith et al., 2009) was thresholded above 3.719, corresponding to $P < 0.0001$, to maintain a z-map that featured only the main regions of the DMN (i.e. posterior cingulate cortex/precuneus, medial prefrontal cortex, inferior parietal lobules, lateral temporal cortices; Fig. 5A). Resting state data were processed in raw data units using the MIT Connectivity Toolbox (CONN; RRID:SCR_009550). The data processing pipeline featured registration of T1-weighted anatomical data to the functional dataset for each participant, realignment and reslicing of functional data, identification of movement artifacts using the Artifact Detection Tools (ART; RRID:SCR_005994) and movement thresholds equal to voxel width. Anatomical data were segmented using the 'New Segmentation' algorithm (SPM12; RRID:SCR_007037). Functional data were denoised via regression of mean white matter signal, mean cerebrospinal fluid signal, 24 Volterra expansion movement parameters and scan-nulling regressors (Lemieux et al., 2007) produced by ART. Additional processing was implemented via a combination of specialized open-source software tools. SyGN (Avants et al., 2008; Avants et al., 2010; Tustison and Avants, 2013) from the Advanced normalization Tools (ANTs; version 2.x, committed in January 2016; http://stnava.github.io/ANTs/; RRID:SCR_004757; Avants et al., 2009) was used to compute neuroanatomically plausible symmetric diffeomorphic matrices and transform each subject's anatomical data to the ICBM MNI brain template that features sharp resolution, detailed gyrification and high signal-to-noise ratio, while minimizing abnormal anatomy biases (Fonov et al., 2011). The cranium of the ICBM template had been removed in advance,

similarly as for the anatomical data, prior to the normalization of datasets. Normalized resolution was limited to $3 \times 3 \times 3\,mm^3$ due to restrictions posed by computational demands. Functional data were filtered using a temporal highpass filter with a cutoff frequency of 1/90 Hz, smoothed with a 3D Gaussian kernel of 6 mm FWHM and subjected to the computationally intensive Eigenvector Centrality Mapping (ECM; Lohmann et al., 2010; Wink et al., 2012) using the Leipzig Image Processing and Statistical Inference Algorithms (LIPSIA; version 2.2.7 – released in May 2011; Max Planck Institute for Human Cognitive and Brain Sciences, Leipzig, Germany; http://www.cbs.mpg.de/institute/software/lipsia; RRID:SCR_009595; Lohmann et al., 2000), similarly to previous studies (Koelsch and Skouras, 2014; Taruffi et al., 2017; Skouras et al., 2019). ECM was preferred over other methods because it as an assumption-free, data-driven approach with solid grounding on advanced graph theory that effectively reflects patterns of whole-brain functional connectomics (Borgatti, 2005; Bonacich and Lloyd, 2004; Lohmann et al., 2010; Wink et al., 2012). To enable parametric testing, ECM z-maps were gaussianized (Albada and Robinson, 2007) and subjected to statistical tests as described in the section 'Statistical analysis'.

2.6. Code accessibility

All original code developed for the analysis has been made available to any researcher for purposes of reproducing or extending the analysis, via the 'NKI_RS_analysis' public repository (GitHub; RRID:SCR_002630; https://git.io/vxddl). Following download, the main analysis and progressive output can be viewed on any browser (HTML version) or replicated and modified interactively using the Live Editor in Matlab v 9.3 or higher (MLX version).

2.7. Data accessibility

Neuroimaging data, further described in (McDonald et al., 2017), are available online via the Neuroimaging Informatics Tools Resources Clearinghouse (NITRC; RRID:SCR_003430). Diagnostic assessment data are available following the completion of a data transfer agreement with the Nathan Kline Institute (Nathan S. Kline Institute for Psychiatric Research; New York; USA, RRID:SCR_004334) via the Collaborative Informatics and Neuroimaging Suite Data Exchange (COINS; Mind Research Network RRID:SCR_000805).

2.8. Statistical analysis

Standard general linear modeling was employed to quantify NF performance and learning. Using Pearson's r as a metric of similarity, actual NF moment-to-moment regulation, as captured by the angular position of a needle on a tachometer-like NF display (Fig. 2B), was compared to a linear vector representing the target performance of the experimental design (Fig. 2C), producing a measure of NF performance for each of the 12 experimental trials. For each participant, average NF scores were computed separately for DMN up-regulation trials (wander), and DMN down-regulation trials (focus), in each of the two experimental blocks. NF learning score was computed as the improvement in NF regulation from the first to the second block of the session. NF performance score was computed as the average correlation between target performance and actual NF regulation in the second block of the session (following the introductory block of the session which comprised the participants' very first practice experience of NF and of each trial type). Lilliefors test (Lilliefors, 1969) was used to assess normality and Grubbs' test (Grubbs, 1969) was used for outlier detection. Parametric correlation testing was used to assess the relation between DMN up-regulation learning and DMN down-regulation learning score, because the variables were normally distributed. Non-parametric correlation testing was used to assess the relation between overall neurofeedback performance and age, because the distribution of age deviated from normality. Permutation testing was used to assess differences in neurofeedback performance scores between the experimental and control groups. Detailed documentation of the analysis, along with explanatory comments and an interactive program have been made available to facilitate replication and in support of the Open Science Initiative. Five statistical tests were performed in total. To control for *Type I* error due to performing multiple statistical tests using data from the same sample, we used the Bonferonni correction method (Abdi, 2007) and set the adjusted two-tail significance level to $\alpha = 0.005$.

For interpretative purposes and due to previous evidence (Scheinost et al., 2014) we investigated whether our main findings could be

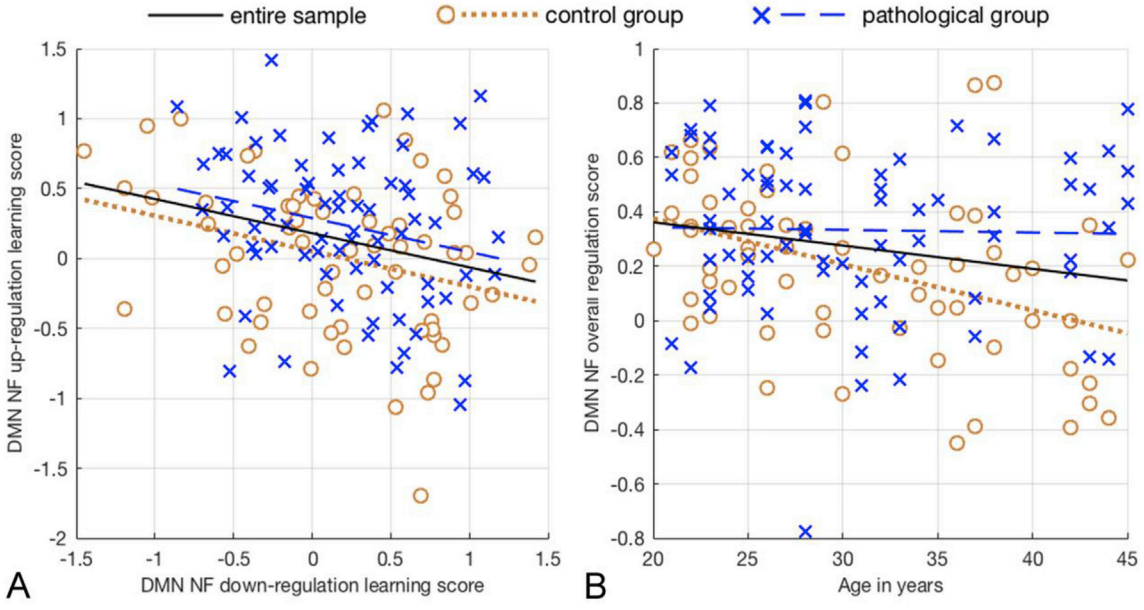

Fig. 3. Illustration of the correlation tests performed.
A, The figure shows lines of best fit for the pathological group (dashed blue line; N = 74), the control group (dotted brown line; N = 62) and the entire sample (black line; N = 136). Default mode network neurofeedback up-regulation and down-regulation learning, are negatively correlated [$r = -0.258$, $R^2 = 0.067$, $p = 0.0024$]. B, Default mode network neurofeedback regulation performance decreases with age only in psychiatrically healthy adults [$r = -0.412$, $R^2 = 0.17$, $p = 0.0009$].

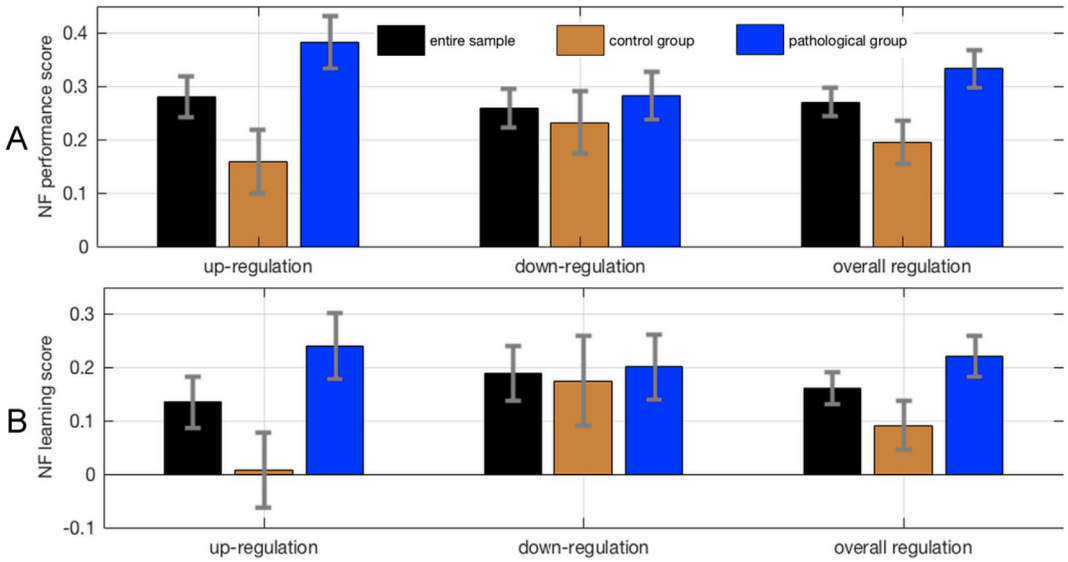

Fig. 4. Neurofeedback scores across experimental groups.
A, Neurofeedback performance and neurofeedback learning scores for up-regulation, down-regulation and overall regulation. Scores are depicted separately for the control group, the pathological group and the entire sample. Error bars represent standard errors. Possible neurofeedback performance scores range from a value of −1 (corresponding to worst possible performance) to a value of 1 (corresponding to best possible performance). **B**, Possible neurofeedback learning scores range from a value of −2 (corresponding to worsening performance) to a value of 2 (corresponding to maximal learning).

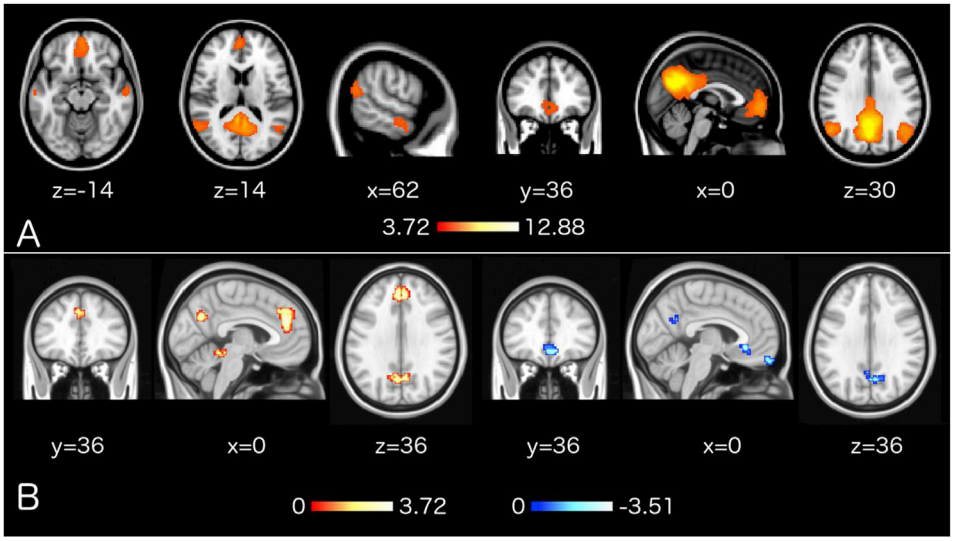

Fig. 5. Pre-NF resting state results.
A, Thresholded version ($z > 3.72$) of the DMN template (Smith et al., 2009) that was used for SVR training prior to neurofeedback. For interpretative purposes, the same template was used for network of interest analyses on pre-NF resting state acquisitions. **B**, Correlations between ECM during pre-NF resting state acquisitions and subsequent neurofeedback learning scores, corrected for whole-brain multiple comparisons using 10,000 Monte Carlo permutations ($z > 2.3$; $P < 0.05$). EC in red-yellow clusters correlated positively with up-regulation learning and EC in blue-white clusters correlated negatively with down-regulation learning. Colormap values are in z-scores and coordinates in MNI space.

supported by pre-NF resting state DMN connectivity. The general systematic approach was to attempt to replicate effects on neurofeedback performance with respective effects involving average pre-NF DMN Eigenvector Centrality (EC). With regards to EC, small-volume analyses, were followed by voxel-wise second-level GLM, to exclude the possibility of subregion-specific effects within the DMN. All voxel-wise tests were corrected for multiple comparisons at $P < 0.05$ using 10,000 Monte Carlo permutations with a cluster forming threshold set to $z > 2.3$, similarly to previous studies (Lohmann et al., 2010; Nierhaus et al., 2015). Regarding the relation between DMN up-regulation learning and DMN down-regulation learning scores, we performed correlation tests between average pre-NF DMN metrics and self-regulation learning scores, separately for up-regulation and down-regulation. Neurofeedback learning scores had been orthogonalised in relation to age and the experimental group factor, to utilize the entire sample while controlling for the influence of these variables, using the recursive Gram-Schmidt orthogonalisation of basis function implemented in SPM12.

3. Results

3.1. Direction of regulation

Lilliefors testing (Lilliefors, 1969) showed that NF up-regulation learning and down-regulation learning scores did not deviate from normality. Further quality assurance using Grubbs' test for outlier detection (Grubbs, 1969) showed that no outliers were present in any utilized variables. Parametric correlation testing revealed that DMN NF up-regulation learning ($M = 0.135$, $SD = 0.554$, $N = 136$) and down-regulation learning scores ($M = 0.189$, $SD = 0.587$) were significantly negatively correlated, with a weak association explaining approximately 7% of the variance, $r(136) = -0.258$, $R^2 = 0.067$, $P = 0.0024$; Fig. 3A.

Controlling for the effects of age and pathology, average pre-NF DMN EC did not correlate with NF up-regulation, nor down-regulation, $P > 0.05$. Voxel-wise GLM, corrected for multiple comparisons using

10,000 Monte Carlo permutations, showed that pre-NF resting state EC in the Posterior Cingulate Cortex (PCC) and Precuneus (PCu) correlated positively with up-regulation learning [$r(136) = 0.989$, $R^2 = 0.978$, $P < 0.00001$ uncorrected; Fig. 5B; Table 2] and negatively with down-regulation learning [$r(136) = -0.986$, $R^2 = 0.972$, $P < 0.00001$ uncorrected; Fig. 5B; Table 3]. Apart from the PCC/PCu, two additional clusters, in the anterior cingulate cortex and cerebellum correlated positively with up-regulation learning, and two other clusters, in the subgenual anterior cingulate cortex and medial prefrontal cortex, correlated negatively with down-regulation learning; Tables 2 and 3. Supplementary 3D neuroimaging data include MNI-registered NIfTI images of these results for visualization and usage as regions of interest in future studies.

3.2. Age

Lilliefors testing showed that the distribution of age ($M = 30.71$ years, $SD = 7.28$, $N = 136$) deviated from normality. Non-parametric correlation testing using Spearman's correlation coefficient revealed that in the pathological group, age ($M = 30.70$ years; $SD = 7.17$; $n_a = 74$) had no effect on overall neurofeedback performance ($M = 0.333$, $SD = 0.301$), $r(74) = -0.0711$, $P = 0.547$. In the control group, age ($M = 30.71$ years; $SD = 7.48$; $n_b = 62$) correlated negatively with overall DMN NF performance score ($M = 0.195$, $SD = 0.312$) with a moderate association that explained 17% of the variance, $r(62) = -0.412$, $R^2 = 0.17$, $P = 0.0009$; Fig. 3B.

Age did not correlate significantly with average pre-NF DMN EC, in neither the pathological nor the control group, ($P > 0.05$). Voxel-wise GLM, corrected for multiple comparisons using 10,000 Monte Carlo permutations, revealed that age had distinct effects in the two groups on resting state functional connectomics, however these effects were not localized within the DMN (Supplementary Figs. S1–S2; Supplementary Tables 1–2). Supplementary 3D neuroimaging data include MNI-registered NIfTI images of these results for visualization and usage as regions of interest in future studies.

3.3. Psychiatric pathology

Non-parametric independent samples t-tests, with 100,000 permutations per test, revealed that participants with a psychiatric history performed significantly better in DMN NF up-regulation ($M = 0.383$, $SD = 0.420$, $n_a = 74$) than the control group ($M = 0.159$, $SD = 0.467$, $n_b = 62$), $t(134) = -2.951$, $P = 0.0036$; $d = 0.504$; Fig. 4A. Down-regulation performance was not significantly different between participants with a psychiatric history ($M = 0.283$, $SD = 0.385$) and the control group ($M = 0.232$, $SD = 0.462$), $t(134) = -0.711$, $P = 0.479$. The difference in up-regulation performance was due to a lack of learning, with regards to up-regulation (mind-wandering), in the control group; Fig. 4B.

An ROI analysis of DMN EC, using gaussianized ECM z-maps revealed marginally higher DMN EC in the pathological group, $t(134) = 1.884$, $p = 0.031$, $d = 0.324$. Voxel-wise GLM, corrected for multiple comparisons using 10,000 Monte Carlo permutations, revealed ECM differences between the two groups, however these effects were not localized within the DMN (Supplementary Fig. S3; Supplementary Table 3). Supplementary 3D neuroimaging data include MNI-registered NIfTI images of these results for visualization and usage as regions of interest in future studies. Neurofeedback scores across diagnostic categories are displayed in Fig. 6.

4. Discussion

In relation to existing questions of fundamental importance to self-regulating brain function, we have shown that initial learning of DMN self-regulation is influenced by age and psychiatric history, as well as by pre-NF differences in EC. Specifically, during an initial, brief DMN rt-fMRI NF session, participants with a psychiatric history outperform healthy controls in DMN up-regulation. Further, age correlates negatively with the ability to self-regulate DMN function, in healthy, young adults. Finally, up-regulation learning and down-regulation learning scores are negatively correlated in both patients and healthy controls and partly determined by pre-NF EC of the PCC/PCu.

A negative effect of age on DMN self-regulation is not surprising, given that reduced connectivity within the DMN's PCC and medial prefrontal cortex has been observed in normal aging (Andrews-Hanna et al., 2010; Sambataro et al., 2010), due to decreasing DMN integrity (Dennis and Thompson, 2014). The DMN also comprises the primary locus of earliest amyloid deposition due to aging in cognitively normal individuals (Dennis and Thompson, 2014; Palmqvist et al., 2017). Although it does not affect cognitive performance, such a neurobiological burden poses limitations on the neural efficiency of the DMN, leading to functional connectivity changes (Palmqvist et al., 2017) and age-related decline in task-related modulation of DMN activity (Sambataro et al., 2010). Our finding indicates that in healthy subjects, age explains 17% of the variation in NF self-regulation scores. This strong effect is even more remarkable considering that the age range in our study was limited to young adults (20–45 years of age), similarly to most NF studies to date. Hence, age must be considered and explicitly modeled when assessing the ability to self-regulate brain function.

Although no previous rt-fMRI study investigated age effects on rt-fMRI NF performance, our finding corroborates complementary evidence, regarding self-regulation, from electrophysiological biofeedback and neurofeedback studies. Heart rate variability biofeedback performance has been reported to correlate negatively with age and the effects of biofeedback self-regulation training on cardiovascular measures were less pronounced in older subjects (Lehrer et al., 2006). EEG theta amplitude up-regulation was also illustrated to be noticeably better in young compared to old subjects, although that study did not investigate performance differences between age groups via statistical testing (Wang and Hsieh, 2013).

DMN activity has been linked primarily to occipital alpha band activity (Jann et al., 2010) that is known to decrease with age (Breslau et al., 1989), substantiating a plausible physiological basis for the effects observed here. It should be noted that despite the evidence for decreased self-regulation performance in older subjects, the beneficial effects of neurofeedback and biofeedback self-regulation training on cognitive and respiratory function, are stronger in elders (Lehrer et al., 2006; Wang and Hsieh, 2013), suggesting the suitability of self-regulation training as a promising intervention to support healthy aging.

A surprising finding from our study relates to the absence of an age effect in the pathological group. In cohort with the complementary finding of better performance in the pathological group, our results suggest that good self-regulation performance is not necessarily reflecting healthy brain function. Our results imply that higher up-regulation performance in the pathological group was likely due to higher ECM in the DMN at baseline, especially because higher ECM in the DMN at baseline was also associated with better up-regulation learning. This corroborates previous evidence of pathologically altered DMN function (Broyd et al., 2009) and may be associated to reduced DMN coherence due to increased DMN connectivity with the rest of the brain. Indeed our

Table 2
Correlations between ECM during resting state and subsequent neurofeedback up-regulation learning. Up-regulation learning scores, had been orthogonalised with regards to age and psychiatric pathology, to control for confounding effects. Results are corrected for whole-brain multiple comparisons using 10,000 Monte Carlo permutations ($z > 2.3$, $P < 0.05$). The outermost right column indicates the maximal z-value of voxels within a cluster (with the mean z-value of all voxels within a cluster in parentheses). Abbreviations: ACC: Anterior Cingulate Cortex; PCC: Posterior Cingulate Cortex; PCu: Precuneus.

	MNI coord.	cluster size (mm^3)	z-value: max (mean)
ACC	−3 39 28	4320	3.73 (2.74)
PCC/PCu	6 −63 34	1620	3.21 (2.62)
Cerebellum	−6 −42 −11	729	3.05 (2.62)

Table 3
Correlations between ECM during resting state and subsequent neurofeedback down-regulation learning. Down-regulation learning scores, had been orthogonalised with regards to age and psychiatric pathology, to control for confounding effects. Results are corrected for whole-brain multiple comparisons using 10,000 Monte Carlo permutations ($z > 2.3$, $P < 0.05$). The outermost right column indicates the maximal z-value of voxels within a cluster (with the mean z-value of all voxels within a cluster in parentheses). Abbreviations: PCC: Posterior Cingulate Cortex; PCu: Precuneus; mPFC: medial Prefrontal Cortex; sACC: subgenual Anterior Cingulate Cortex.

	MNI coord.	cluster size (mm^3)	z-value: max (mean)
PCC/PCu	3 −63 25	1053	−2.82 (−2.46)
sACC	−3 27 −2	1026	−3.15 (−2.61)
mPFC	12 54 −17	1107	−3.51 (−2.78)

ECM results suggest that the DMN is more interconnected with the rest of the brain in the pathological group and in this sense less coherent as an independent resting state network. These new findings suggest that generic hypotheses of reduced performance and reduced connectivity in pathological populations need to be revisited.

It is worth considering that the capacity to show improvement in NF performance is contingent upon aberrant baseline activity. That is, when NF is used to normalize brain activity in patients that present moderately abnormal, aberrant activity, the patients will probably perform better than controls that present normal, stable activity patterns. On the other hand, in the face of severe pathology that impairs fundamental learning capacities, the ability to improve NF performance will be impaired as well, although this was not the case for the high-functioning pathological group of the present study.

The third important finding of our study is that initial learning of DMN self-regulation is unidirectional, with the amount of learning in one direction of regulation opposing learning in the other direction of regulation and explaining 7% of its variation. In this study, up-regulation was associated with mind-wandering strategies and down-regulation with focusing attention. Thus, our findings suggest that learning to self-regulate depends on task-specific performance constraints rather than a more generic ability to self-regulate. This may partly explain why the search for general predictors of successful neurofeedback learning has not been successful so far and why the proportion of up to 30% of participants that fail to self-regulate effectively, even following extensive practice (Harmelech et al., 2015), varies between targeted brain regions and paradigms (Sitaram et al., 2017). In order to design improved experimental and clinical protocols, it is critical to consider the direction of regulation, task-specific peculiarities, and individual predispositions such as pre-NF functional connectomics in target regions.

It remains possible that the present findings may be influenced by unaccounted factors that are not homogeneously distributed across the two experimental groups or across the age range of the sample. These may include experience with types of training that can exert a covert influence on the ability to self-regulate physiological processes; e.g. meditational practice, musical training, acting experience etc. (Gruzelier, 2014a; 2014b). It is possible that, on average, the pathological group had received more training in self-regulation of cognitive and physiological functions through participation in cognitive behavioral therapy programs. Moreover, it remains possible that our findings are limited only to the DMN and only to initial sessions of self-regulation. Future research should systematically investigate learning effects in cardinal brain networks (i.e. default mode, executive control and salience networks) across several sessions using identical protocols.

A potential experimental limitation is that even though focusing was meant to drive down-regulation of the DMN, focusing on thoughts of personal relevance, such as auto-biographical events or autobiographical planning can lead to increased DMN activity (Gusnard et al., 2001; Addis et al., 2007; Spreng and Grady, 2010; Spreng et al., 2015) and that we did not possess quantifiable information on the extent of focusing on such thoughts across participants. Therefore, it cannot be ascertained that the observed effects are not partly attributable to structured variation in the level of focusing on self-oriented thoughts. Arguably, clinical populations and especially patients with major depressive disorder, spend an increased amount of time performing mind-wandering and self-referential rumination, compared to non-clinical populations. This may result in enhancing the ability to up-regulate the DMN and suggests that appropriately designed DMN NF paradigms may serve in producing clinically relevant neuromarkers. On the other hand, in contrast to task-fMRI paradigms that elicit DMN activation, in the context of neurofeedback tasks and with the aid of real-time neurofeedback displays, participants learn to avoid using mental strategies with negative impact on the neurofeedback performance. Moreover, the ability of both groups to improve on down-regulation (focusing) supports that they did not

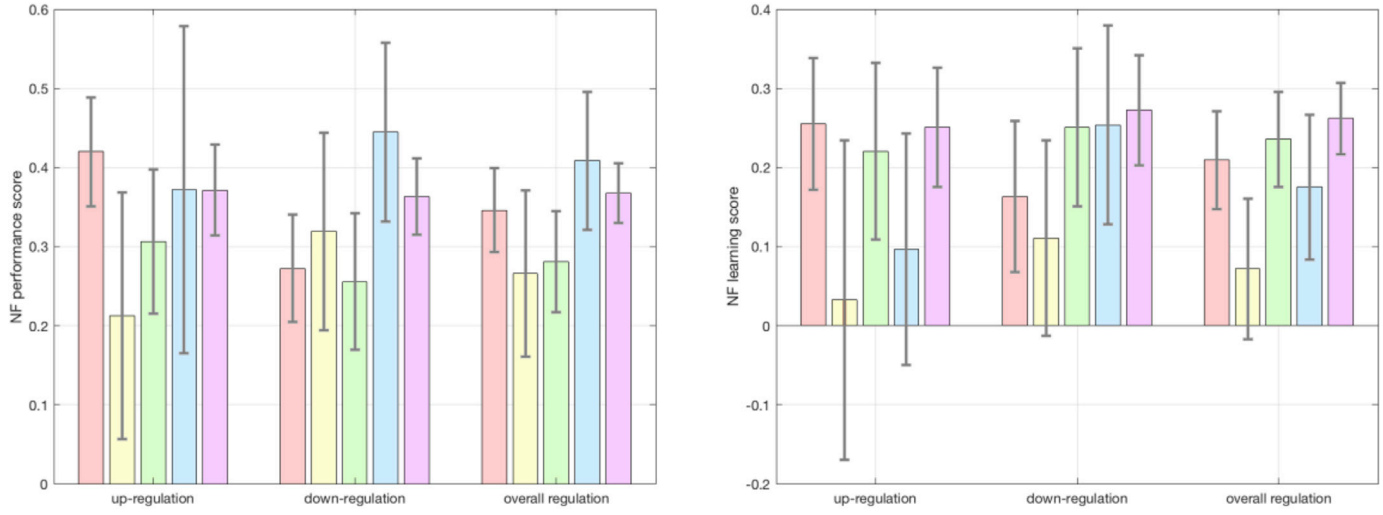

Fig. 6. Neurofeedback scores across diagnostic categories.
A, Neurofeedback performance and neurofeedback learning scores for up-regulation, down-regulation and overall regulation. Scores are depicted sequentially, from left to right, for affective disorders, ADHD, anxiety disorders, eating disorders and substance abuse. Error bars represent standard errors. Possible neurofeedback performance scores range from a value of −1 (corresponding to worst possible performance) to a value of 1 (corresponding to best possible performance). **B**, Possible neurofeedback learning scores range from a value of −2 (corresponding to worsening performance) to a value of 2 (corresponding to maximal learning). Color coding is in concordance with Fig. 1: pink ~ affective disorders; yellow ~ ADHD; green ~ anxiety disorders; blue ~ eating disorders; purple ~ substance use disorder.

differ in terms of the level of self-referential cognition during focus trials (Fig. 4B). Nevertheless, the level of self-referential thinking should be quantified and modeled in future DMN NF studies. Moreover, future studies on the self-regulation of the DMN, should consider using different or complementary instructions that relate down-regulation to attending to one's immediate environment and up-regulation to internally mediated cognition. Such studies could aid in clarifying the specificity and inter-individual variability of DMN functions.

In conclusion, we have illustrated that participants with a psychiatric history can perform better than healthy controls in self-regulating brain function. The ability to up-regulate brain function appears to decrease with age only in the absence of psychiatric history, and good performance in learning to up-regulate the DMN through one cognitive task does not imply equally good performance in down-regulating the DMN through another cognitive task. The latter is evidenced by the negative correlation between up-regulation learning and down-regulation learning, which are partly explained by PCC/PCu functional connectomics during resting state. Although it remains to be determined to what extent these findings are specific to the DMN and to initial sessions of self-regulation through rt-fMRI NF, our findings contribute to the furtherment of neurophysiological knowledge and our understanding of the neural mechanisms underpinning self-regulation of brain function specifically. We anticipate that our findings will solidify the foundations for more systematic modeling of the self-regulation of brain function and assist in the design of advanced technologies and experimental protocols for clinical applications.

Acknowledgements

This work was supported by the European Union's Horizon 2020 research and innovation programme under the Marie Sklodowska-Curie action grant agreement No 707730, the Foundation for Research in Science and the Humanities at the University of Zurich (STWF-17-012), the Baugarten Stiftung, and the Swiss National Science Foundation (BSSG10_155915, 32003B_166566). Principal support for the Rockland Sample Real-Time Neurofeedback project was provided by the NIMH BRAINS R01-MH101555 (PI Craddock). The authors thank Cameron Craddock for insightful discussions. The authors declare no competing financial interests.

Appendix A. Supplementary data

Supplementary data to this article can be found online at https://doi.org/10.1016/j.neuroimage.2019.05.008.

References

Abdi, H., 2007. Bonferroni and Šidák corrections for multiple comparisons. Encycl. Meas. Stat. 3, 103—107.
Addis, D.R., Wong, A.T., Schacter, D.L., 2007. Remembering the past and imagining the future: common and distinct neural substrates during event construction and elaboration. Neuropsychologia 45 (7), 1363–1377.
Albada, V.S., Robinson, P.A., 2007. Transformation of arbitrary distributions to the normal distribution with application to EEG test–retest reliability. J. Neurosci. Methods 161, 205–211.
Andrews-Hanna, J.R., Reidler, J.S., Sepulcre, J., Poulin, R., Buckner, R.L., 2010. Functional-anatomic fractionation of the brain's default network. Neuron 65 (4), 550–562.
Avants, B.B., Epstein, C.L., Grossman, M., Gee, J.C., 2008. Symmetric diffeomorphic image registration with cross-correlation: evaluating automated labeling of elderly and neurodegenerative brain. Med. Image Anal. 12, 26–41.
Avants, B.B., Tustison, N., Song, G., 2009. Advanced normalization tools (ANTS). Insight 2, 1–35.
Avants, B., Tustison, N., Song, G., Cook, P., Klein, A., Gee, J., 2010. A reproducible evaluation of ANTs similarity metric performance in brain image registration. Neuroimage 54, 2033–2044.
Benedek, M., Jauk, E., Beaty, R.E., Fink, A., Koschutnig, K., Neubauer, A.C., 2016. Brain mechanisms associated with internally directed attention and self-generated thought. Sci. Rep. 6, 22959.
Binder, J.R., Desai, R.H., Graves, W.W., Conant, L.L., 2009. Where is the semantic system? A critical review and meta-analysis of 120 functional neuroimaging studies. Cerebr. Cortex 19 (12), 2767–2796.
Borgatti, S.P., 2005. Centrality and network flow. Soc. Network. 27, 55–71.
Bonacich, P., Lloyd, P., 2004. Calculating status with negative relations. Soc. Network. 26 (4), 331–338.
Brakowski, J., Spinelli, S., Dorig, N., Bosch, O.G., Manoliu, A., Holtforth, M.G., Seifritz, E., 2017. Resting state brain network function in major depression - depression symptomatology, antidepressant treatment effects, future research. J. Psychiatr. Res. 92, 147–159.
Breslau, J., Starr, A., Sicotte, N., Higa, J., Buchsbaum, M.S., 1989. Topographic EEG changes with normal aging and SDAT. Electroencephalogr. Clin. Neurophysiol. 72, 281–289.
Mugler, J.P., Brookeman, J.R., 1990. Three-dimensional magnetization-prepared rapid gradient-echo imaging (3D MP RAGE). Magn. Reson. Med. 15 (1), 152–157.
Broyd, S.J., Demanuele, C., Debener, S., Helps, S.K., James, C.J., Sonuga-Barke, E.J.S., 2009. Default-mode brain dysfunction in mental disorders: a systematic review. Neurosci. Biobehav. Rev. 33, 279–296.
Cox, R.W., Jesmanowicz, A., Hyde, J.S., 1995. Real-time functional magnetic resonance imaging. Magn. Reson. Med. 33, 230–236.
Cox, R.W., 1996. Afni software for analysis and visualization of functional magnetic resonance neuroimages. Comput. Biomed. Res. 29, 162–173.
Craddock, C.R., Milham, M.P., LaConte, S.M., 2013. Predicting intrinsic brain activity. Neuroimage 82, 127–136.
Damoiseaux, J.S., Beckmann, C.F., Arigita, E.J.S., Barkhof, F., Scheltens, P., Stam, C.J., Smith, S.M., Rombouta, S.A.R.B., 2008. Reduced resting-state brain activity in the 'default network' in normal aging. Cerebr. Cortex 18, 1856–1864.
deCharms, R.C., Maeda, F., Glover, G.H., Ludlow, D., Pauly, J.M., Soneji, D., Gabrieli, J.D.E., Mackey, S.C., 2005. Control over brain activation and pain learned by using real-time functional MRI. Proc. Natl. Acad. Sci. U. S. A. 102, 18626–18631.
Dennis, E.L., Thompson, P.M., 2014. Functional brain connectivity using fMRI in aging and Alzheimer's disease. Neuropsychol. Rev. 24, 49–62.
Emmert, K., Kopel, R., Sulzer, J., Brühl, A.B., Berman, B.D., Linden, D.E.J., Horovitz, S.G., Breimhorst, M., Caria, A., Frank, S., Johnston, S., Long, Z., Paret, C., Robineau, F., Veit, R., Bartsch, A., Beckmann, C.F., Van De Ville, D., Haller, S., 2016. Meta-analysis of real-time fMRI neurofeedback studies using individual participant data: how is brain regulation mediated? Neuroimage 124, 806–812.
Engen, H.G., Kanske, P., Singer, T., 2017. The neural component-process architecture of endogenously generated emotion. Soc. Cognit. Affect Neurosci. 12 (2), 197–211.
Faul, F., Erdfelder, E., Lang, A.G., Buchner, A., 2007. G*Power 3: a flexible statistical power analysis program for the social, behavioral, and biomedical sciences. Behav. Res. Methods 39, 175–191.
Faul, F., Erdfelder, E., Buchner, A., Lang, A.G., 2009. Statistical power analyses using G*Power 3.1: tests for correlation and regression analyses. Behav. Res. Methods 41, 1149–1160.
Fonov, V., Evans, A.C., Botteron, K., Almli, R.C., McKinstry, R.C., Collins, L.D., 2011. Unbiased average age-appropriate atlases for pediatric studies. Neuroimage 54, 313–327.
Fox, P.T., Lancaster, J.L., 2002. Mapping context and content: the BrainMap model. Nat. Rev. Neurosci. 3, 319–321.
Greve, D.N., Fischl, B., 2009. Accurate and robust brain image alignment using boundary-based registration. Neuroimage 48, 63–72.
Griswold, M.A., Jakob, P.M., Heidemann, R.M., Nittka, M., Jellus, V., Wang, J., Kiefer, B., Haase, A., 2002. Generalized autocalibrating partially parallel acquisitions (grappa). Magn. Reson. Med. 47, 1202–1210.
Grubbs, F., 1969. Procedures for detecting outlying observations in samples. Technometrics 11, 1–21.
Gusnard, D.A., Akbudak, E., Shulman, G.L., Raichle, M.E., 2001. Medial prefrontal cortex and self-referential mental activity: relation to a default mode of brain function. Proc. Natl. Acad. Sci. U.S.A. 98 (7), 4259–4264.
Gruzelier, J.H., 2014a. EEG-neurofeedback for optimising performance. I: a review of cognitive and affective outcome in healthy participants. Neurosci. Biobehav. Rev. 44, 124–141.
Gruzelier, J.H., 2014b. EEG-neurofeedback for optimising performance. II: creativity, the performing arts and ecological validity. Neurosci. Biobehav. Rev. 44, 142–158.
Haller, S., Birbaumer, N., Veit, R., 2010. Real-time fMRI feedback training may improve chronic tinnitus. Eur. Radiol. 20, 696–703.
Hamilton, J.P., Farmer, M., Fogelman, P., Gotlib, I.H., 2015. Depressive rumination, the default-mode network, and the dark matter of clinical neuroscience. Biol. Psychiatry 78, 224–230.
Harmelech, T., Friedman, D., Malachvolume, R., 2015. Differential magnetic resonance neurofeedback modulations across extrinsic (visual) and intrinsic (default-mode) nodes of the human cortex. J. Neurosci. 35, 2588–2595.
Harmelech, T., Preminger, S., Wertman, E., Malach, R., 2013. The day-after effect: long term, Hebbian-like restructuring of resting-state fMRI patterns induced by a single epoch of cortical activation. J. Neurosci. 33, 9488–9497.
Hartwell, K.J., Prisciandaro, J.J., Borckardt, J., Li, X.B., George, M.S., Brady, K.T., 2013. Real-Time fMRI in the treatment of nicotine dependence: a conceptual review and pilot studies. Psychol. Addict. Behav. 27, 501–509.
Heberle, H., Meirelles, G.V., da Silva, F.R., Telles, G.P., Minghim, R., 2015. InteractiVenn: a web-based tool for the analysis of sets through Venn diagrams. BMC Bioinf. 16, 169.
Jann, K., Kottlow, M., Dierks, T., Boesch, C., Koenig, T., 2010. Topographic electrophysiological signatures of fMRI resting state networks. PLoS One 5, e12945.
Jenkinson, M., Smith, S., 2001. A global optimisation method for robust affine registration of brain images. Med. Image Anal. 5, 143–156.
Jenkinson, M., Bannister, P., Brady, M., Smith, S., 2002. Improved optimization for the robust and accurate linear registration and motion correction of brain images. Neuroimage 17, 825–841.

Joachims, T., 1999. Making large-scale SVM learning practical. In: Schölkopf, B., Burges, C., Smola, A. (Eds.), Advances in Kernel Methods - Support Vector Learning. MIT Press.
Kelly, A.M., Uddin, L.Q., Biswal, B.B., Castellanos, F.X., Milham, M.P., 2008. Competition between functional brain networks mediates behavioral variability. Neuroimage 39, 527–537.
Koelsch, S., Skouras, S., 2014. Functional centrality of amygdala, striatum and hypothalamus in a "small-world" network underlying joy: an fMRI study with music. Hum. Brain Mapp. 35 (7), 3485–3498.
Konishi, M., McLaren, D.G., Engen, H., Smallwood, J., 2015. Shaped by the past: the default mode network supports cognition that is independent of immediate perceptual input. PLoS One 10 (6), e0132209.
Krieger-Redwood, et al., 2016. Down but not out in posterior cingulate cortex: deactivation yet functional coupling with prefrontal cortex during demanding semantic cognition. Neuroimage 141, 366–377.
LaConte, S.M., Strother, S.C., Cherkassky, V., Anderson, J., Hu, X., 2005. Support vector machines for temporal classification of block design fmri data. Neuroimage 26, 317–329.
LaConte, S.M., Peltier, S.J., Hu, X.P., 2007. Real-time fmri using brain-state classification. Hum. Brain Mapp. 28, 1033–1044.
Laird, A., Lancaster, J., Fox, P., 2005. BrainMap. The social evolution of a human brain mapping database. Neuroinformatics 3, 65–77.
Lehrer, P., Vaschillo, E., Lu, S.E., Eckberg, D., Vaschillo, B., Scardella, A., Habib, R., 2006. Heart rate variability biofeedback: effects of age on heart rate variability, baroreflex gain, and asthma. Chest 129, 278–284.
Lemieux, L., Salek-Haddadi, A., Lund, T.E., Laufs, H., 2007. Modelling large motion events in fMRI studies of patients with epilepsy. Magn. Reson. Imag. 25, 894–901.
Li, X., Hartwell, K.J., Borckardt, J., Prisciandaro, J.J., Saladin, M.E., Morgan, P.S., Johnson, K.A., LeMatty, T., Brady, K.T., George, M.S., 2013. Volitional reduction of anterior cingulate cortex activity produces decreased cue craving in smoking cessation: a preliminary real-time fMRI study. Addict. Biol. 18, 739–748.
Liew, S.L., Rana, M., Cornelsen, S., de Barros, M.F., Birbaumer, N., Sitaram, R., Cohen, L.G., Soekadar, S.R., 2016. Improving motor corticothalamic communication after stroke using real-time fMRI connectivity-based neurofeedback. Neurorehabilitation Neural Repair 30, 671–675.
Lilliefors, H., 1969. On the Kolmogorov–Smirnov test for the exponential distribution with mean unknown. J. Am. Stat. Assoc. 64, 387–389.
Linden, D.E.J., Habes, I., Johnston, S.J., Linden, S., Tatineni, R., Subramanian, L., Sorger, B., Healy, D., Goebel, R., 2012. Real-time self-regulation of emotion networks in patients with depression. PLoS One 7, e38115.
Lohmann, G., Müller, K., Bosch, V., Mentzel, H., Hessler, S., 2000. LIPSIA-leipzig Image Processing and Statistical Inference Algorithms.
Lohmann, G., Margulies, D.S., Horstmann, A., Pleger, B., Lepsien, J., Goldhahn, D., et al., 2010. Eigenvector centrality mapping for analyzing connectivity patterns in fMRI data of the human brain. PLoS One 5, e10232.
Mayer, J.S., Roebroeck, A., Maurer, K., Linden, D.E.J., 2010. Specialization in the default mode: task-induced brain deactivations dissociate between visual working memory and attention. Hum. Brain Mapp. 31, 126–139.
McDonald, A.R., et al., 2017. The real-time fMRI neurofeedback based stratification of Default Network Regulation Neuroimaging data repository. Neuroimage 146, 157–170.
Megumi, F., Yamashita, A., Kawato, M., Imamizu, H., 2015. Functional MRI neurofeedback training on connectivity between two regions induces long-lasting changes in intrinsic functional network. Front. Hum. Neurosci. 9, 160.
Mulders, P.C., van Eijndhoven, P.F., Schene, A.H., Beckmann, C.F., Tendolkar, I., 2015. Resting-state functional connectivity in major depressive disorder: a review. Neurosci. Biobehav. Rev. 56, 330–344.
Murphy, C., et al., 2017. Fractionating the anterior temporal lobe: MVPA reveals differential responses to input and conceptual modality. Neuroimage 147, 19–31.
Murphy, C., et al., 2018. Distant from input: evidence of regions within the default mode network supporting perceptually-decoupled and conceptually-guided cognition. Neuroimage 171, 393–401.
Nierhaus, T., et al., 2015. Imperceptible somatosensory stimulation alters sensorimotor background rhythm and connectivity. J. Neurosci. 35 (15), 5917–5925.
Nooner, K.B., et al., 2012. The NKI-Rockland sample: a model for accelerating the pace of discovery science in psychiatry. Front. Neurosci. 6, 152.
Palmqvist, S., Schöll, M., Strandberg, O., Mattsson, N., Stomrud, E., Zetterberg, H., Blennow, K., Landau, S., Jagust, W., Hansson, O., 2017. Earliest accumulation of β-amyloid occurs within the default-mode network and concurrently affects brain connectivity. Nat. Commun. 8, 1214.
Raichle, M.E., MacLeod, A.M., Snyder, A.Z., Powers, W.J., Gusnard, D.A., Shulman, G.L., 2001. A default mode of brain function. Proc. Natl. Acad. Sci. U. S. A. 98, 676–682.
Robineau, F., Saj, A., Neveu, R., Van De Ville, D., Scharnowski, F., Vuilleumier, P., 2017. Using real-time fMRI neurofeedback to restore right occipital cortex activity in patients with left visuo-spatial neglect: proof-of-principle and preliminary results. Neuropsychol. Rehabil. 1–22.
Rugg, M.D., Vilberg, K.L., 2013. Brain networks underlying episodic memory retrieval. Curr. Opin. Neurobiol. 23 (2), 255–260.
Sambataro, F., Murty, V.P., Callicott, J.H., Tan, H., Das, S., Weinberger, D.R., Mattay, V.S., 2010. Age-related alterations in default mode network: impact on working memory performance. Neurobiol. Aging 31, 839–852.
Scheinost, D., Stoica, T., Wasylink, S., Gruner, P., Saksa, J., Pittenger, C., Hampson, M., 2014. Resting state functional connectivity predicts neurofeedback response. Front. Behav. Neurosci. 338.
Scott, A., Courtney, W., Wood, D., de la Garza, R., Lane, S., King, M., Wang, R., Roberts, J., Turner, J.A., Calhoun, V.D., 2011. Coins: an innovative informatics and neuroimaging tool suite built for large heterogeneous datasets. Front. Neuroinf. 5.
Shehzad, Z., Giavasis, S., Li, Q., Benhajali, Y., Yan, C., Yang, Z., Milham, M., Bellec, P., Craddock, R.C., 2015. The preprocessed connectomes project quality assessment protocol - a resource for measuring the quality of mri data. Front. Neurosci. 9.
Sitaram, R., Ros, T., Stoeckel, L., Haller, S., Scharnowski, F., Lewis-Peacock, J., Weiskopf, N., Blefari, M.L., Rana, M., Oblak, E., Birbaumer, N., Sulzer, J., 2017. Closed-loop brain training: the science of neurofeedback. Nat. Rev. Neurosci. 18, 86–100.
Skouras, S., Falcon, C., Tucholka, A., Rami, L., Sanchez-Valle, R., Llado, A., Gispert, J.D., Molinuevo, J.L., 2019. Mechanisms of functional compensation, delineated by eigenvector centrality mapping, across the pathophysiological continuum of Alzheimer's disease. Neuroimage: Clinic 22, 101777.
Smith, S.M., Fox, P.T., Miller, K.L., Glahn, D.C., Fox, P.M., Mackay, C.E., Filippini, N., Watkins, K.E., Toro, R., Laird, A.R., Beckmann, C.F., 2009. Correspondence of the brain's functional architecture during activation and rest. Proc. Natl. Acad. Sci. U. S. A. 106, 13040–13045.
Spreng, R.N., Grady, C.L., 2010. Patterns of brain activity supporting autobiographical memory, prospection, and theory of mind, and their relationship to the default mode network. J. Cogn. Neurosci. 22 (6), 1112–1123.
Spreng, R.N., DuPre, E., Selarka, D., Garcia, J., Gojkovic, S., Mildner, J., Turner, G.R., et al., 2014. Goal-congruent default network activity facilitates cognitive control. J. Neurosci. 34 (42), 14108–14114.
Spreng, R.N., Gerlach, K.D., Turner, G.R., Schacter, D.L., 2015. Autobiographical planning and the brain: activation and its modulation by qualitative features. J. Cogn. Neurosci. 27 (11), 2147–2157.
Stoeckel, L.E., et al., 2014. Optimizing real time fMRI neurofeedback for therapeutic discovery and development. Neuroimage Clin. 5, 245–255.
Straw, A.D., 2008. Vision egg: an open-source library for realtime visual stimulus generation. Front. Neuroinf. 2, 4.
Subramanian, L., Hindle, J.V., Johnston, S., Roberts, M.V., Husain, M., Goebel, R., Linden, D., 2011. Real-time functional magnetic resonance imaging neurofeedback for treatment of Parkinson's Disease. J. Neurosci. 31, 16309–16317.
Taruffi, L., Pehrs, C., Skouras, S., Koelsch, S., 2017. Effects of sad and happy music on mind-wandering and the default mode network. Sci. Rep. 7 (1), 14396.
Turner, D.C., Robbins, T.W., Clark, L., Aron, A.R., Dowson, J., Sahakian, B.J., 2003. Cognitive enhancing effects of modafinil in healthy volunteers. Psychopharmacology 165 (3), 260–269.
Tustison, N.J., Avants, B.B., 2013. Explicit B-spline regularization in diffeomorphic image registration. Front. Neuroinf. 7, 39.
Van De Ville, D., Jhooti, P., Haas, T., Kopel, R., Lovblad, K., Scheffler, K., Haller, S., 2012. Recovery of the default mode network after demanding neurofeedback training occurs in spatio-temporally segregated subnetworks. Neuroimage 63, 1775–1781.
Vatansever, D., Menon, D.K., Manktelow, A.E., Sahakian, B.J., Stamatakis, E.A., 2015. Default mode network connectivity during task execution. Neuroimage 122, 96–104.
Wang, J.R., Hsieh, S., 2013. Neurofeedback training improves attention and working memory performance. Clin. Neurophysiol. 124, 2406–2420.
Weissman, D.H., Roberts, K.C., Visscher, K.M., Woldorff, M.G., 2006. The neural bases of momentary lapses in attention. Nat. Neurosci. 9, 971–978.
Wink, A.M., de Munck, J.C., van der Werf, Y.D., van den Heuvel, O.A., Barkhof, F., 2012. Fast eigenvector centrality mapping of voxel-wise connectivity in functional magnetic resonance imaging: implementation, validation, and interpretation. Brain Connect. 2 (5), 265–274.
Whitfield-Gabrieli, S., Ford, J.M., 2012. Default mode network activity and connectivity in psychopathology. Annu. Rev. Clin. Psychol. 8, 49–76.
Wood, D., King, M., Landis, D., Courtney, W., Wang, R., Kelly, R., Turner, J.A., Calhoun, V.D., 2014. Harnessing modern web application technology to create intuitive and efficient data visualization and sharing tools. Front. Neuroinf. 8.
Young, K.D., Siegle, G.J., Zotev, V., Phillips, R., Misaki, M., Yuan, H., Drevets, W.C., Bodurka, J., 2017. Randomized clinical trial of real-time fMRI amygdala neurofeedback for major depressive disorder: effects on symptoms and autobiographical memory recall. Am. J. Psychiatry 174, 748–755.
Young, K.D., Zotev, V., Phillips, R., Misaki, M., Yuan, H., Drevets, W.C., Bodurka, J., 2014. Real-time FMRI neurofeedback training of amygdala activity in patients with major depressive disorder. PLoS One 9, e88785.
Zhang, Y., Brady, M., Smith, S., 2001. Segmentation of brain mr images through a hidden markov random field model and the expectation-maximization algorithm. IEEE Trans. Med. Imaging 20, 45–57.
Zhang, D., Raichle, M.E., 2010. Disease and the brain's dark energy. Nat. Rev. Neurol. 6, 15–28.